Optically field-ionized He plasmas

A. Egbert, D. M. Simanovskii,* B. N. Chichkov,† and B. Wellegehausen
Institut für Quantenoptik, Universität Hannover Welfengarten 1, D-30167 Hannover, Germany
(Received 21 January 1998)

Time resolved XUV radiation of He plasmas produced by optical field ionization in an intense laser field is studied. Fast and slow line emission components generated due to different pumping mechanisms are observed. It is shown that the intensities of these components can be manipulated by varying the laser frequency and polarization. Amplification on the 3-2 transition ($\lambda = 164$ nm) of He II ions is demonstrated. [S1063-651X(98)12606-5]

PACS number(s): 52.50.Jm, 52.25.−b, 42.55.Lt, 42.55.Vc

I. INTRODUCTION

With ultrashort pulse laser systems a strongly nonequilibrium plasma can be produced by optical field ionization (OFI) of a gaseous medium in an intense laser field. The stage of ionization and the electron temperature of this OFI plasma can be controlled by the parameters of the laser pulse, which allows one to create favorable conditions for the realization of soft-x-ray lasers. In fact, first successful demonstrations of amplification and soft-x-ray lasing in OFI plasmas have already been reported [1–6].

Since the interest directed towards producing coherent x rays from OFI plasmas continues to grow, detailed experimental investigations of these plasmas are important. For this goal spectroscopic methods are usually applied. Taking into account the transient nature of OFI plasmas, it is desirable to make measurements with temporal resolution. Up to now in most experiments only time-integrated spectra have been recorded. Theoretical interpretations of these spectra neglecting the transient nature of OFI plasmas remain uncertain. There are only a few examples where time-resolved measurements of OFI plasma radiation have been performed [7–9]. In [7] the 13.5 nm Lyman-α emission of a lithium plasma has been studied. A 20 ps delay of the Lyman-α line with respect to the pump pulse and a 20 ps pulse width have been observed. In [8] the time-dependent electron velocity distribution in tunnel ionized He plasmas has been investigated. It has been found that the He II Lyman-α line dominates the spectrum at times later than 400 ps after the laser pulse. In [9] the emission of helium and nitrogen plasmas has been studied in a temporal window of about 3 ns duration. It has been observed that the He II Lyman-α emission has an initial spike followed later by a slow revival of radiation, which is confirmed by our observations.

In this paper we present results of time-resolved spectroscopic investigations of optically field-ionized He plasmas in a very broad temporal window of 500 ns. We observe fast and slow line emission components in the Lyman and Balmer series of He II ions and show how the intensities of these components can be manipulated. We provide explanations of our results and demonstrate amplification on the Balmer-α transition ($\lambda = 164$ nm). In Sec. II, a general discussion of OFI plasmas is given. In Sec. III, the experimental setup is described. In Sec. IV, experimental results and necessary explanations are given.

II. PARAMETERS OF OFI PLASMAS

It is well known that in an intense laser field ionization occurs in the tunneling regime when the condition $\gamma = (E_i/2U_p)^{1/2} < 1$ is fulfilled. Here γ is the Keldysh parameter [10], E_i and $U_p = 9.33\times10^{-14} I\lambda^2$ are the ionization and ponderomotive potentials (in eV), I (in W/cm^2) and λ (in μm) are the laser intensity and wavelength. The required laser intensity I_Z for producing an ion with the charge Z (the so-called appearance intensity) is well predicted by the barrier-suppression model [11], $I_Z = 4.0\times10^9 E_i^4/Z^2$ W/cm^2. The reason this simple model works so well is discussed in the Appendix. The Keldysh parameter calculated at the appearance intensity, $\gamma = \gamma_Z$, and the condition for tunnel ionization can be written as

$$\gamma_Z = 8Z\omega(\mathcal{R}/E_i^3)^{1/2} = 0.73(Z/\lambda)(\mathcal{R}/E_i)^{3/2} < 1, \qquad (1)$$

where $\mathcal{R} = 13.6$ eV, $\omega = 1.24/\lambda$ is the laser frequency (in eV), and λ is in μm. For He the appearance intensities are $I_1 \simeq 1.5\times10^{15}$ W/cm^2 (He$\rightarrow$He$^+$) and $I_2 \simeq 9\times10^{15}$ W/cm^2 (He$^+\rightarrow$He^{2+}).

The electron distribution function after tunnel ionization ($X^{Z-1}\rightarrow X^Z$) in a linearly polarized laser field is given by (see [4,12,13] for details) $f(\mathbf{p})d^3\mathbf{p} = f(p_\parallel)f(\mathbf{p}_\perp)dp_\parallel d^2\mathbf{p}_\perp$, where

$$f(p_\parallel) = (2\pi m T_{Z\parallel})^{-1/2}\exp\left(-\frac{p_\parallel^2}{2mT_{Z\parallel}}\right),$$
$$f(\mathbf{p}_\perp) = (2\pi m T_{Z\perp})^{-1}\exp\left(-\frac{\mathbf{p}_\perp^2}{2mT_{Z\perp}}\right) \qquad (2)$$

are the one-dimensional and the two-dimensional Maxwellian distributions in directions $\parallel$ and $\perp$ to the laser field. The corresponding electron temperatures (in eV) are

*Present address: A. F. Ioffe Institute of Physics and Technology, Polytehnicheskaya 26, St. Petersburg, Russia.
†Permanent address: P. N. Lebedev Physics Institute, Leninsky prospect 53, Moscow, Russia.

$$T_{Z\parallel}=\frac{3\omega}{2\gamma^3},\quad T_{Z\perp}=\frac{\omega}{2\gamma}. \tag{3}$$

It is natural [4] to estimate these temperatures at the ion appearance intensity. In this case we obtain

$$T_{Z\parallel}=\frac{3\omega}{2\gamma_Z^3}=4.8(E_i/\mathcal{R})^{9/2}\lambda^2/Z^3,$$
$$T_{Z\perp}=\frac{\omega}{2\gamma_Z}=0.85(E_i/\mathcal{R})^{3/2}/Z. \tag{4}$$

These estimates are very reliable and have the same accuracy as the ion appearance intensity (see Appendix). For He and $\lambda=0.8$ μm Eqs. (4) give $T_{1,2\parallel}=44$ and 197 eV and $T_{1,2\perp}=2$ and 3.4 eV. For the second harmonic, $\lambda=0.4$ μm, $T_{1,2\parallel}=11$ and 49 eV and $T_{1,2\perp}$ are the same.

Below we are interested in the average electron temperature T, which characterizes the OFI plasmas after relaxation (due to electron-electron collisions) of the temperature anisotropy,

$$T=\frac{1}{3Z}\sum_{i=1}^{Z}(T_{i\parallel}+2T_{i\perp})\simeq\frac{1}{Z}\sum_{i=1}^{Z}\frac{\omega}{2\gamma_i^3}$$
$$=1.6(\lambda^2/Z)\sum_{i=1}^{Z}(E_i/\mathcal{R})^{9/2}/i^3. \tag{5}$$

Here we take into account that $T_\parallel\gg T_\perp$ is usually fulfilled. For the above example, He and $\lambda=0.8$ μm, $T\simeq40$ eV is obtained. This electron temperature is in a very good agreement with experimental data [14] and calculations [15]. For the second harmonic $T\simeq10$ eV.

After tunnel ionization in a circularly polarized laser field with intensity I^c the average energy of released electrons $\mathcal{E}_{\rm av}$ is determined by [16] $\mathcal{E}_{\rm av}=U_p^c=9.33\times10^{-14}I^c\lambda^2$. Using $I_Z^c\simeq6\times10^9E_i^4/Z^2$ for the ion appearance intensity (see Appendix) and $T=2\mathcal{E}_{\rm av}/3$ for the average electron temperature, we obtain

$$T=\frac{1}{Z}\sum_{i=1}^{Z}T_i=12.8(\lambda^2/Z)\sum_{i=1}^{Z}(E_i/\mathcal{R})^4/i^2. \tag{6}$$

For He and $\lambda=0.8$ μm, $T_1=87$ eV, $T_2=524$ eV, and $T=306$ eV, in good agreement with experimental data [17].

In Eqs. (5) and (6) the spatial variation of the laser intensity is neglected, i.e., it is assumed that the laser intensity is constant in the focal plane. In general, one should take into account volume effects. For a Gaussian laser beam tightly focused into a center of a gaseous medium with a length $2L$, the volume V_i, where each atom loses i or more electrons, is given by [11]

$$V_i=\pi w_0^2z_R\left\{\frac{4c_i}{3}+\frac{2c_i^3}{9}-\frac{4}{3}\arctan(c_i)\right\}, \tag{7}$$

where w_0 is the radius of the focused beam, z_R is the Rayleigh length, I_0 is the peak intensity, $c_i=(I_0/I_i-1)^{1/2}$, and I_i is the corresponding ion appearance intensity. This expression is valid when $L\geqslant z_Rc_i$ is fulfilled. In the opposite case, $L<z_Rc_i$, which is not considered in [11], the volume V_i, where the peak laser intensity exceeds I_i, is

$$V_i=\pi w_0^2L\left\{(1+L^2/3z_R^2)\ln\left(\frac{I_0/I_i}{1+L^2/z_R^2}\right)\right.$$
$$\left.+\frac{4}{3}\left[1-\frac{z_R}{L}\arctan(L/z_R)\right]+\frac{2L^2}{9z_R^2}\right\}. \tag{8}$$

In the weak focusing limit $L\ll z_R$, Eq. (8) reduces to the expression $V_i=\pi w_0^2L\ \ln(I_0/I_i)$, which can be easily obtained without integration.

Taking into account volume effects, the average electron temperature can be written as

$$T=\frac{\Sigma_iV_iT_i}{\Sigma_iV_i}, \tag{9}$$

where V_i are given by Eqs. (7) and (8), T_i is given by Eq. (6) for the circular polarization, and $T_i=\omega/2\gamma_i^3$ for the linear polarization. This temperature is usually lower than is given by Eqs. (5) and (6). Under our experimental conditions, volume effects are more important for the circular polarization (due to higher ion appearance intensities). In this case, the average electron temperature will be reduced to ~150 eV. Concluding this section we emphasize that the OFI electron temperatures can be estimated with a very good accuracy without computer simulations.

III. EXPERIMENTAL SETUP

Two experimental setups that have been used for investigations of optically field-ionized (OFI) He plasmas are shown in Fig. 1. The plasma is produced by focusing of 150 fs Ti:sapphire laser pulses (BMI model Alpha 10A) into He gas jets. Linearly or circularly polarized laser pulses at 800 nm and at the second harmonic (400 nm) with the energy of 100 mJ or 60 mJ are used.

He gas is injected into the vacuum chamber (10^{-5} Torr) by a pulsed nozzle (General Valve Corporation, model Iota One), with an opening time of about 1 ms. The experiments are performed at backing pressures of 0.1–1.5 bar, which correspond to particle densities of 10^{17}–10^{18} cm^{-3} in the interaction region.

For investigations of temporal dynamics of He OFI plasmas a single jet nozzle with an output diameter of 0.3 mm is used. In this case [see Fig. 1(a)] the plasma emission is observed at a small angle to the direction of the laser beam. This is necessary to protect our registration system from direct laser radiation. Time-resolved XUV spectra are obtained with a grating monochromator (Jobin Yvon, LHT 30, 550 lines/mm gold grating, angle of incidence 19°) equipped with a fast microchannel plate (MCP) detector having a 1 ns temporal resolution. The signals are recorded by a digitizing oscilloscope (Tektronix, model TDS 620B, 2.5 gigasamples/s, 500 MHz) and averaged over 100 laser shots. Due to the small plasma size and large distances between the He II spectral lines, it is possible to operate the XUV monochromator without an entrance slit. The monochromator is

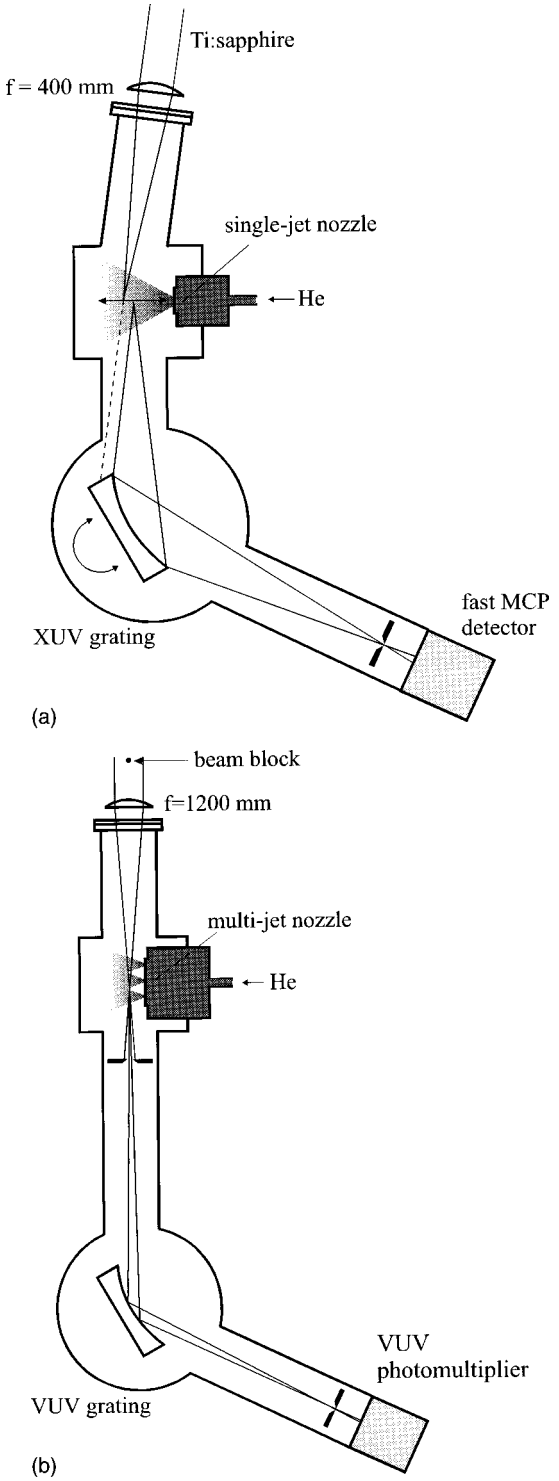

FIG. 1. Experimental setups used for time-resolved investigations of He plasmas (a) and for investigations of amplification on the Balmer-α transition (b).

adjusted so that the OFI plasma is produced at a distance from the grating corresponding to the position of the entrance slit [see Fig. 1(a)]. This setup provides high illumination strength and allows one to investigate the spatial distribution of the plasma emission at a certain wavelength by rotating the grating.

To study a possibility of amplification on the Balmer-α transition ($\lambda = 164$ nm) the experimental arrangement shown

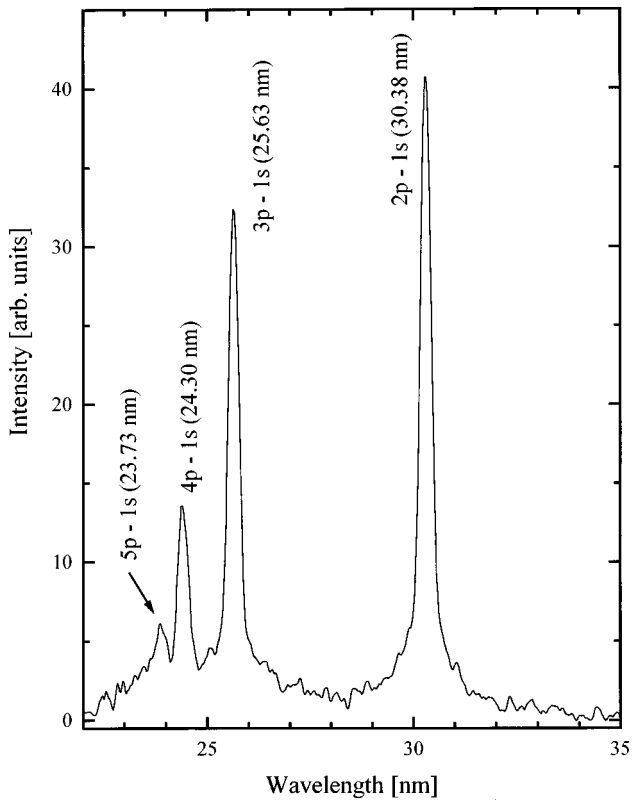

FIG. 2. Typical time-integrated spectrum of a He II OFI plasma.

in Fig. 1(b) is used. In this case the nozzle has six output holes with a diameter of 0.3 mm. The distance between the hole centers is 0.5 mm. A certain number of these holes can be opened and closed by a mechanical shutter that provides a possibility for a variation of the plasma length. In these experiments a focusing lens with $f = 1200$ cm is used to produce a 4 mm long homogeneous plasma column. In front of the focusing lens a narrow central part of the laser beam is blocked to protect our monochromator from the direct laser radiation. A shadow produced by this 2 mm beam block allows one to reduce the laser intensity on the entrance slit by two orders of magnitude. The signals at 164 nm are detected by a VUV photomultiplier with a CsI photocathode and recorded by a digitizing oscilloscope.

IV. RESULTS AND DISCUSSIONS

In this section results of experimental investigations of He OFI plasmas are discussed. For a reference, a typical time-integrated spectrum of a He II OFI plasma is shown in Fig. 2. This spectrum is recorded in the direction of the laser beam with a single shot grazing incidence spectrometer (McPherson, model 248/310-G) with MCP intensifier and charge-coupled device array as a detector.

Time-resolved investigations of He II OFI plasma radiation are performed with the experimental setup shown in Fig. 1(a). The plasma is produced by focusing of 150 fs Ti:sapphire laser pulses with an energy of 60 mJ into He gas jets at backing pressures of 100–500 mbar. The estimated intensity in the focus, $I_0 \simeq 2 \times 10^{16}$ W/cm^2, is high enough to completely strip the He atoms.

Typical oscillograms of the He II Lyman-α and Lyman-β line emission are shown in Fig. 3. Fast and slow line emission components can be clearly seen. The time duration of

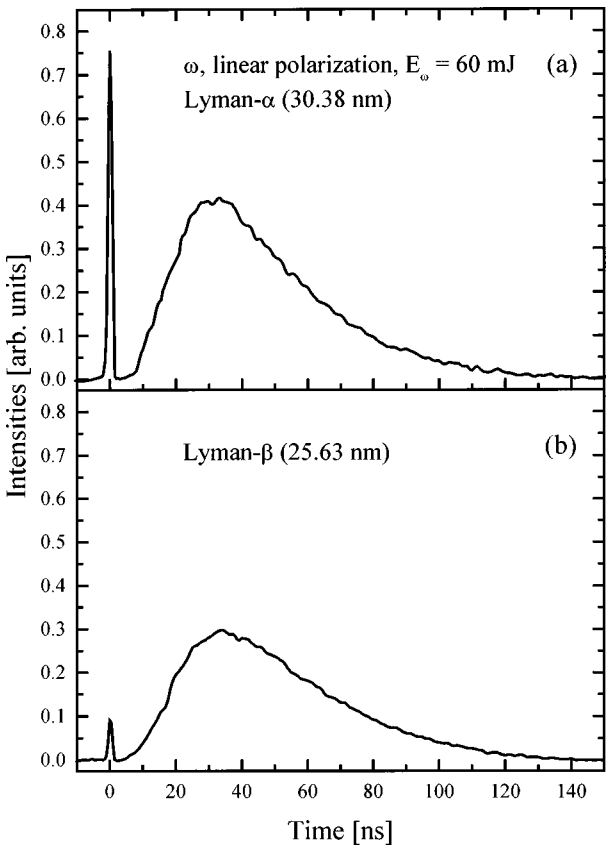

FIG. 3. Time-resolved He II Lyman-α (a) and Lyman-β (b) line emission.

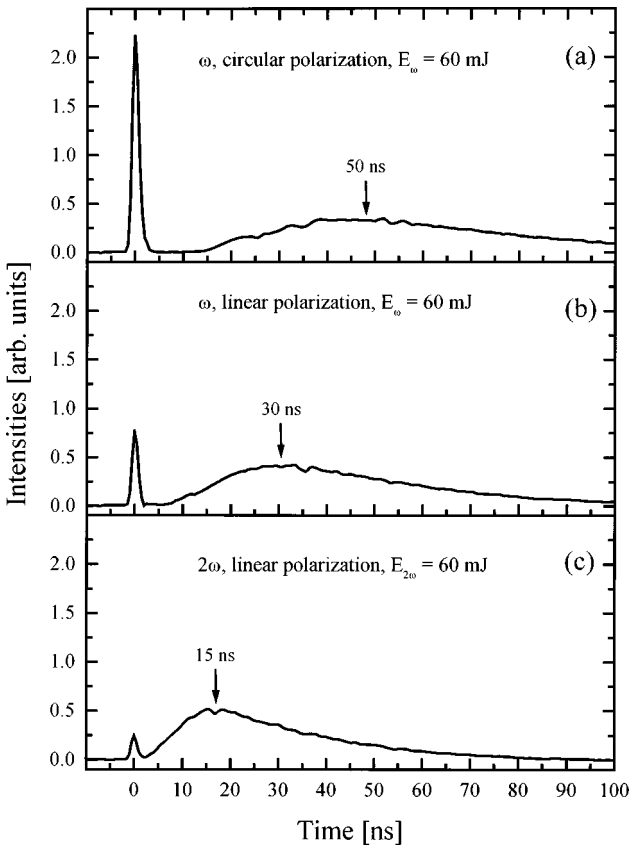

FIG. 5. Time-resolved radiation of the He II Lyman-α line from OFI plasmas produced by circularly (a) and linearly (b) polarized laser pulses, and by second harmonic radiation (c).

the fast component is below the 1 ns resolution limit of our detector and has not been resolved. The slow component reaches its maximum value after a 30 ns delay with respect to the laser pulse. During this time a considerable expansion and cooling of the OFI plasma occurs. Therefore, it is reasonable to assume that the slow component originates due to three-body recombination. The recombination signals for both lines are comparable. The fast component signal for the Lyman-β line is much weaker than the corresponding signal for the Lyman-α line. For the Lyman-γ line the fast component signal reduces further and follows the n^{-5} scaling law with the main quantum number. This behavior can be explained by electron impact excitation from the ground state of He^+ ions, which are produced at the outer region of the OFI plasma channel. A small fraction of the He^+ ions can also be left in the region where He^{2+} ions are generated. A self-termination of the fast component signal with time can be explained by the electron impact ionization of He^+ ions after the laser pulse ($He^+ \rightarrow 0$) and/or by the reduction of the number of hot electrons due to the relaxation of the electron temperature anisotropy ($e^-_{hot} \rightarrow 0$).

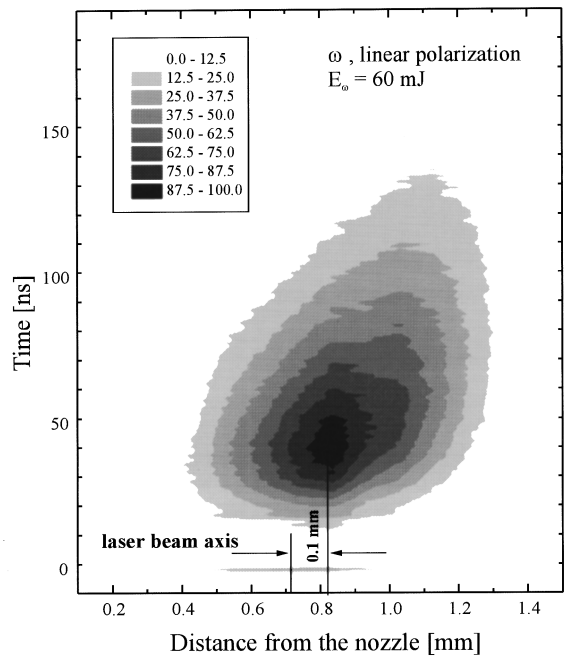

FIG. 4. Spatial distribution of the Lyman-β line emission at 300 mbar backing pressure.

The spatial distribution of the Lyman-β line emission is illustrated in Fig. 4. This distribution is obtained with the XUV monochromator operating without an entrance slit [see Fig. 1(a)] by rotating the grating. Our setup allows one to get a resolution of 200 μm. Due to the time delay between the slow and fast components the maximum of the recombination signal is spatially shifted with respect to the laser beam axis. The value of this shift is determined by the gas jet expansion velocity.

Parameters of the fast (excitation) and slow (recombination) components depend on the laser polarization and wavelength. In Fig. 5 the temporal evolution of the He II Lyman-

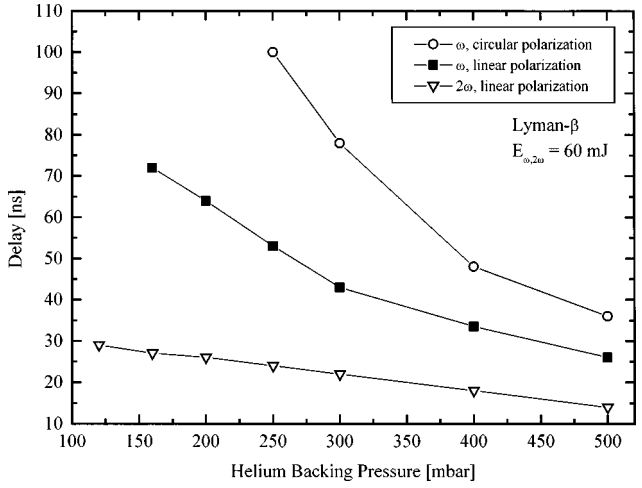

FIG. 6. Dependences of the time delay between the slow and fast components on the He backing pressure for Lyman-β radiation.

α line is demonstrated for circularly and linearly polarized laser pulses, and for the second harmonic (linear polarization). As can be seen, the fast component signal is the strongest for the circular polarization. In this case the OFI electrons are very hot and collisional excitation is effective. The self-termination of the fast component signal occurs due to the ionization of He^+ ions. For the second harmonic the fast component signal is weak. The sufficiently hot electrons (for collisional excitation of He^+ ions) exist only when the OFI electron distribution remains anisotropic, i.e., during the time interval $t \leqslant \tau_{ee}$, where τ_{ee} is the electron thermalization time. In this case the self-termination of the fast component is explained by $e^-_{\rm hot} \rightarrow 0$.

As can be seen in Fig. 5, the slow component is stronger and appears earlier in time when the plasma is produced by the second harmonic radiation. This behavior is consistent with the initial OFI plasma temperatures. As it follows from Sec. II of our paper, the average temperatures of the OFI electrons in He plasmas are $\simeq$150 eV for the circular polarization, $\simeq$40 eV for the linear polarization, and $\simeq$10 eV for the second harmonic. In the last case the expansion of the OFI plasma channel starts from the lowest temperature. Therefore, cooling to the electron temperatures of $\leqslant$1 eV, which are necessary for the efficient three-body recombination of He^{2+} ions, occurs faster.

The cylindrical OFI plasma column expands in the ambient gas injected by a pulsed nozzle. This expansion is accompanied by the formation of a strong shock wave propagating into the ambient gas. Adapting a strong shock explosion model [18], the radius of the plasma channel R and the electron temperature T_e can be estimated from

$$\frac{dR}{dt} = \sqrt{\frac{ZT_e}{M_i}} = v_0 \frac{r_0}{R}, \quad T_e = T_0 (r_0/R)^2, \tag{10}$$

where r_0 is the initial plasma radius ($r_0 \simeq 20$ μm in our case), T_0 is the initial average temperature of the OFI electrons, and $v_0 = \sqrt{ZT_0/M_i}$ is the initial speed of sound (Z and M_i are the ion charge and mass). From Eqs. (10) it follows that

$$R = r_0 \left(1 + \frac{2v_0 t}{r_0}\right)^{1/2} \simeq \sqrt{2v_0 r_0 t}, \quad T_e \simeq T_0 \left(\frac{r_0}{2v_0 t}\right), \tag{11}$$

and that the rate of the plasma expansion decreases with time as $dR/dt \sim t^{-1/2}$. Using the average temperatures of the OFI electrons given above and the measured values of the time delay for the slow component (see Fig. 5), electron temperatures corresponding to the three recombination peaks shown in Fig. 5 can be obtained $T_e \simeq 0.3-0.4$ eV.

The time delay between the slow and fast components reduces with the He backing pressure, since the three-body recombination rate rapidly increases ($\sim N_e^2$) with the electron density. This is illustrated in Fig. 6 for the Lyman-β line.

Due to the different density dependences of the excitation and recombination components the ratio between them, R(fast/slow), decreases with the backing pressure; see Fig. 7. In this figure the data obtained with 60 mJ linearly polarized laser pulses at the fundamental frequency are shown. At low backing pressures the fast component signal dominates the spectrum and the slow component gradually disappears.

In Fig. 8 relative populations of the He^+ excited states corresponding to the fast (a) and slow (b) component signals

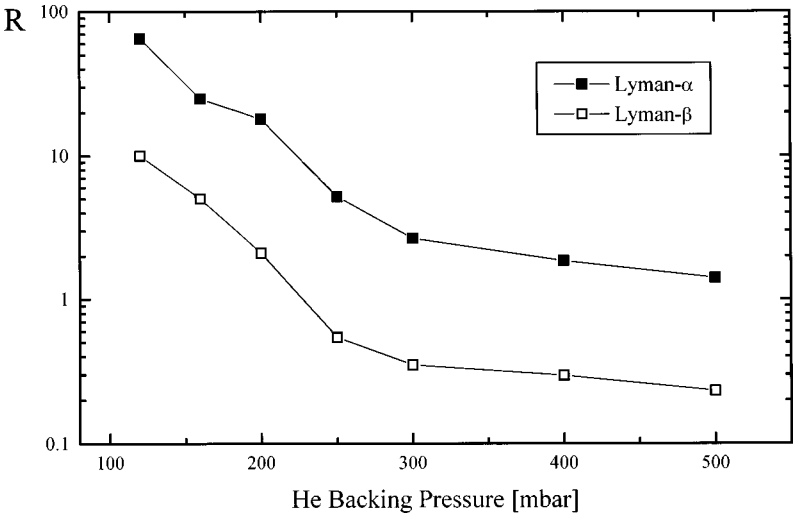

FIG. 7. The ratio between the fast and slow components as a function of the backing pressure. Plasma is produced by 60 mJ linearly polarized laser pulses at the fundamental frequency.

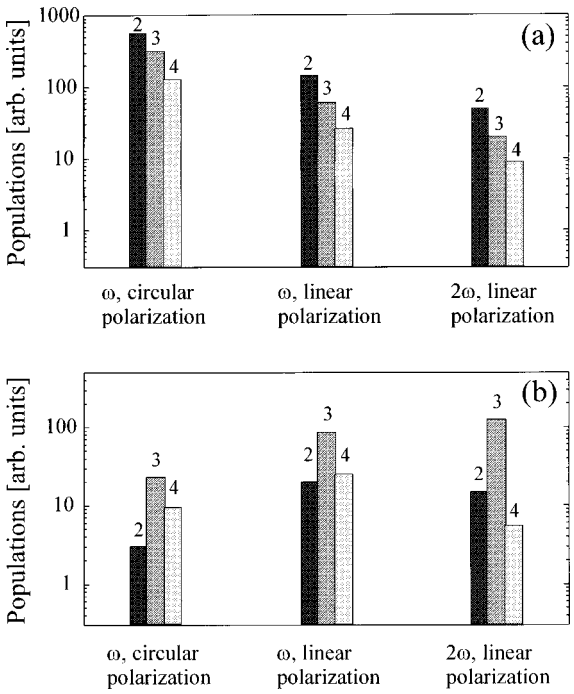

FIG. 8. Relative populations of the excited states of He^+ ions at a backing pressure of 250 mbar: (a) populations corresponding to the fast (excitation) and (b) slow (recombination) components.

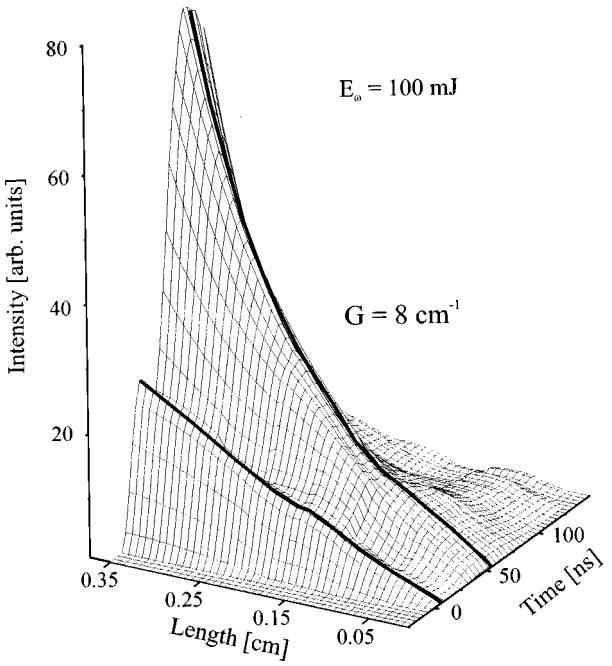

FIG. 9. Variation of the fast and slow component signals with the plasma length at a He backing pressure of 900 mbar. Plasma is produced by 100 mJ linearly polarized laser pulses at the fundamental frequency.

recorded at a 250 mbar backing pressure are shown. These populations are calculated using the following expression $N_{f,s}(n) \sim S_{f,s}/(A_{n,1} g_n)$, where $S_{f,s}$ is the observed signal, $A_{n,1}$ is the radiative decay probability from the level with the main quantum number n to the ground state, and $g_n = 2n^2$ is the statistical weight of this level. It is well known that the electron impact excitation from the ground state of hydrogenlike ions is not able to invert populations of the excited states. Therefore, in the fast (excitation) component no population inversion is observed. Population inversion arises in the cold plasma due to the three-body recombination. This can be seen in Fig. 8(b), which shows that during the three-body recombination stage (slow component) the population inversion is produced on the 3-2, Balmer-α transition. The population inversion is bigger when the plasma is produced by the second harmonic radiation. In this case cooling is faster and the three-body recombination starts at higher electron densities. For the circular polarization, in opposite, cooling and plasma expansion occurs longer. The three-body recombination starts at lower electron densities and the collisional relaxation between the excited states is weaker. In this case a small population inversion can also be observed on the 4-2 transition.

To investigate the possibility of amplification on the Balmer-α transition ($\lambda = 164$ nm) the experimental setup shown in Fig. 1(b) is used. Gain measurements are performed with the gas jet nozzle having six output holes. The length is varied with a mechanical shutter. Due to this the distance between the laser beam focus and the nozzle surface has to be larger than in the previous experiments. Therefore, to obtain the same particle densities with the new setup the backing pressure should be larger.

The variation of the fast and slow component signals with the plasma length is shown in Fig. 9. As can be seen, the fast

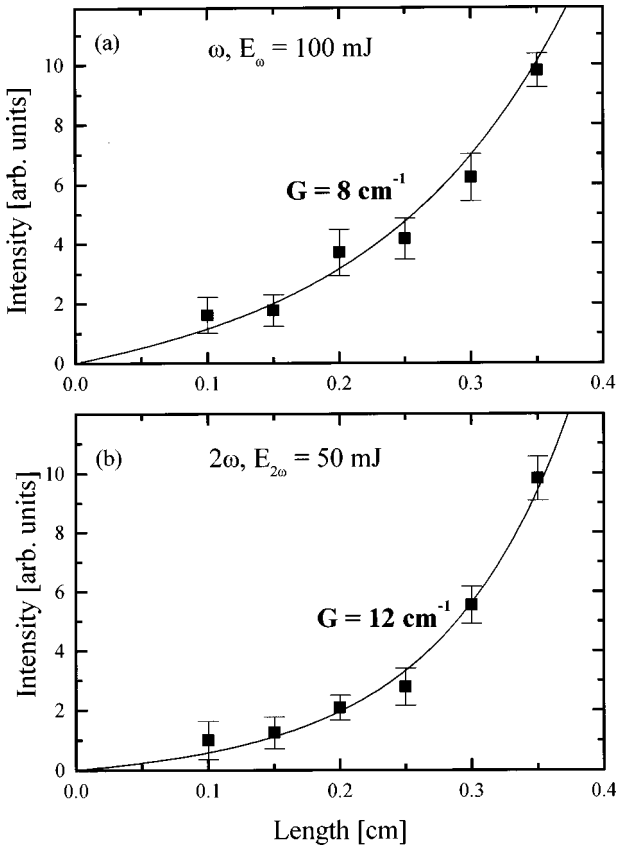

FIG. 10. Dependence of the slow component signal on the plasma length at a He backing pressure of 900 mbar. The plasmas are produced by linearly polarized fundamental (a) and second harmonic (b) laser radiation.

component signal grows linearly with the plasma length, whereas the intensity of the slow component increases exponentially. By fitting these data to the Linford formula [19], a gain coefficient of 8 cm^{-1} is obtained. The gain coefficient is higher ($\simeq 12$ cm^{-1}) when the plasma is created by the second harmonic radiation. Corresponding measurements are illustrated in Fig. 10. Optimum conditions for amplification on the Balmer-α transition occur at the electron densities of $N_e \simeq (0.3-1)\times 10^{16}$ cm^{-3} [20]. These densities are produced due to the cylindrical expansion of the OFI plasma channels. The estimated electron temperatures (see above) are in the range of $0.3-0.4$ eV.

The recombining OFI plasmas are usually considered as good candidates for the realization of soft-x-ray lasers to the ion ground state. Unfortunately, a direct solution of this problem appears difficult due to relatively high OFI electron temperatures. One of the possibilities, which is demonstrated above, is to use excited states for the development of future OFI soft-x-ray lasers. In this case, a rapid cooling of a narrow plasma channel produced in an intense laser field could provide necessary conditions for lasing.

V. CONCLUSION

Time-resolved investigations of He plasmas produced by optical field ionization in an intense laser field have been performed. The nature of the observed fast and slow He^+ line emission components has been studied. Our experimental results allow one to conclude that these emission components originate due to electron impact excitation and three-body recombination, respectively. By varying the laser frequency and polarization, the OFI plasma temperature and the intensities of the fast and slow line emission components can be manipulated. To the best of our knowledge, amplification on the Balmer-α transition ($\lambda = 164$ nm) of He^+ ions has been demonstrated for the first time. These results are important for a better understanding of the OFI plasma properties and the development of future soft-x-ray lasers.

ACKNOWLEDGMENT

This work was supported by the Deutsche Forschungsgemeinschaft.

APPENDIX: WHY THE BARRIER-SUPPRESSION MODEL WORKS SO WELL

The barrier-suppression ionization (BSI) model provides surprisingly good estimates of the ion appearance intensities [11]. Predictions of this model are in a good agreement with experimental results and tunnel-ionization theory [12,21]. Why is it so? The answer to this question is given below.

As follows from the BSI model the atomic electron can freely escape from the Coulomb potential when the laser field strength reaches the critical value $F = Z^3/16n^{*4}$. Here atomic units are used and $n^* = Z(\mathcal{R}/E_i)^{1/2}$ is the effective quantum number. It is remarkable that the same expression for the critical field strength can be obtained from the tunnel-ionization theory.

The probability of tunnel ionization in an intense laser field (for an electron state with a magnetic quantum number $m = 0$) is given by [12,21]

$$W = \omega_a \frac{(2l+1)}{8\pi} \frac{F}{Z} P \left(\frac{4eZ^3}{n^{*4}F} \right)^{2n^*} \exp\left(-\frac{2Z^3}{3n^{*3}F} \right), \tag{A1}$$

where $\omega_a = 4.1\times 10^{16}$ s^{-1} is the atomic frequency, l is the orbital quantum number, F is the laser field amplitude in atomic units, P is a polarization dependent factor [$P = 1$ for a circular polarization and $P = (3Fn^{*3}/\pi Z^3)^{1/2}$ for a linear polarization due to the averaging over a laser field period]. Since the exponential dependence on the laser field strength in Eq. (A1) is determined by the factor

$$\exp\left\{ 2n^* \left[\ln\left(\frac{4eZ^3}{n^{*4}F} \right) - \frac{Z^3}{3n^{*4}F} \right] \right\},$$

it is clear that the tunnel ionization rate becomes appreciable (independent of n^*) when the condition

$$\ln\left(\frac{4eZ^3}{n^{*4}F} \right) - \frac{Z^3}{3n^{*4}F} = 0 \tag{A2}$$

is fulfilled. The solution of the above equation is given by $F = AZ^3/n^{*4}$, where $A = 1/15.34$. This value is very close to the prediction of the BSI model, $A = 1/16$.

In the BSI model the ionization threshold is determined by the electric field amplitude, therefore for a circularly polarized laser field the ion appearance intensity is two times larger as compared to a linear polarization case [22]. We arrive at the same conclusion, if we consider only the exponential dependence of the tunnel ionization probability. Taking the pre-exponential factor into account which is larger for the circular polarization, we obtain the corrected value of the ion appearance intensity $I_Z^c \simeq 1.5 I_Z^l = 6\times 10^9 E_i^4/Z^2$. This expression differs by a factor of 1.5 from the linear polarization case, which is in a good agreement with the experimental observations [22]. Thus, the success of the barrier-suppression model is not fortuitous; it is a signature of the optical field ionization in the tunneling regime.

[1] Y. Nagata, K. Midorikawa, S. Kubodera, M. Obara, H. Tashiro, and K. Toyoda, Phys. Rev. Lett. **71**, 3774 (1993).

[2] B.E. Lemoff, G.Y. Yin, C.L. Gordon III, C.P.J. Barty, and S.E. Harris, Phys. Rev. Lett. **74**, 1574 (1995).

[3] E. Fill, S. Borgström, J. Larsson, T. Starczewski, C.-G. Wahlström, and S. Svanberg, Phys. Rev. E **51**, 6016 (1995).

[4] B.N. Chichkov, A. Egbert, H. Eichmann, C. Momma, S. Nolte, and B. Wellegehausen, Phys. Rev. A **52**, 1629 (1995).

[5] D.V. Korobkin, C.H. Nam, S. Suckewer, and A. Goltsov, Phys. Rev. Lett. **77**, 5206 (1996).

[6] S.M. Hooker, P.T. Epp, and G.Y. Yin, J. Opt. Soc. Am. B **14**, 2735 (1997).

[7] Y. Nagata, K. Midorikawa, S. Kubodera, M. Obara, H. Tashiro, K. Toyoda, and Y. Kato, Phys. Rev. A **51**, 1415 (1995).
[8] T.E. Glover, J.K. Crane, M.D. Perry, R.W. Lee, and R.W. Falcone, Phys. Rev. Lett. **75**, 445 (1995).
[9] S. Borgström, E. Fill, T. Starczewski, J. Steingruber, S. Svanberg, and C.-G. Wahlström, Laser Part. Beams **13**, 459 (1995).
[10] L.V. Keldysh, Zh. Éksp. Teor. Fiz. **47**, 1945 (1964) [Sov. Phys. JETP **20**, 1307 (1965)].
[11] S. Augst, D. Strickland, D.D. Meyerhofer, S.L. Chin, and J.H. Eberly, Phys. Rev. Lett. **63**, 2212 (1989); S. Augst, D.D. Meyerhofer, D. Strickland, and S.L. Chin, J. Opt. Soc. Am. B **8**, 858 (1991).
[12] A.M. Perelomov, V.S. Popov, and M.V. Terent'ev, Zh. Éksp. Teor. Fiz. **50**, 1393 (1966) [Sov. Phys. JETP **23**, 924 (1966)].
[13] N.B. Delone and V.P. Krainov, J. Opt. Soc. Am. B **8**, 1207 (1991).
[14] T.E. Glover, T.D. Donnelly, E.A. Lipman, A. Sullivan, and R. Falcone, Phys. Rev. Lett. **73**, 78 (1994).
[15] T. Ditmire, Phys. Rev. E **54**, 6735 (1996).
[16] P.B. Corkum, N.H. Burnett, and F. Brunel, Phys. Rev. Lett. **62**, 1259 (1989); N.H. Burnett and P.B. Corkum, J. Opt. Soc. Am. B **6**, 1195 (1989).
[17] A. Sagisaka, Y. Nabekawa, K. Kondo, and S. Watanabe, Appl. Phys. B: Lasers Opt. **61**, 217 (1995).
[18] Ya.B. Zel'dovich and Yu.P. Raizer, *Physics of Shock Waves and High Temperature Hydrodynamic Phenomena* (Academic Press, New York, 1966).
[19] G.J. Linford, E.R. Peressini, W.R. Sooy, and M.L. Spaeth, Appl. Opt. **13**, 379 (1974).
[20] M. Villagran and J.J. Rocca, IEEE Trans. Plasma Sci. **18**, 784 (1990).
[21] M.V. Ammosov, N.B. Delone, and V.P. Krainov, Zh. Éksp. Teor. Fiz. **91**, 2008 (1986) [Sov. Phys. JETP **64**, 1191 (1986)].
[22] T. Auguste, P. Monot, L.A. Lompre, G. Mainfray, and C. Manus, J. Phys. B **25**, 4181 (1992); S. Augst and D.D. Meyerhofer, Laser Phys. **4**, 1155 (1994).